

FABRICATING MICROCHANNELS IN ELASTOMER SUBSTRATES FOR STRETCHABLE ELECTRONICS

Michelle C. Yuen

School of Mechanical Engineering
Purdue University
West Lafayette, IN 47907
Email: yuenm@purdue.edu

Rebecca K. Kramer*

School of Mechanical Engineering
Purdue University
West Lafayette, IN 47907
Email: rebeccakramer@purdue.edu

ABSTRACT

As flexible devices and machines become more ubiquitous, there is a growing need for similarly deformable electronics. Soft polymers continue to be widely used as stretchable and flexible substrates for soft electronics, and in particular, soft sensing. These soft sensors generally consist of a highly elastic substrate with embedded microchannels filled with a conductive fluid. Deforming the substrate deforms the embedded microchannels and induces a change in the electrical resistance through the conductive fluid. Microchannels, thus, are the foundation of flexible electronic devices and sensors. These microchannels have been fabricated using various methods, where the manufacturing method greatly impacts device functionality. In this paper, comparisons are made between the following methods of microchannel manufacturing: cast molding, 3D printing of the elastomer substrate itself, and laser ablation. Further processing of the microchannels into flexible electronics is also presented for all three methods. Lastly, recommended ranges of microchannel sizes and their associated reproducibility and accuracy measures for each manufacturing method are presented.

Keywords: additive manufacturing, laser ablation, stretchable electronics, flexible electronics, microchannels

1 Introduction

Soft electronics are advantageous for highly deformable systems. Such systems require flexible materials and components

capable of maintaining their functionality throughout the range of the deformation. In particular, stretchable strain and pressure sensors have applications in highly conformable devices and large deformation systems, such as wearable devices and human-machine interfaces [1–4]. Some of these sensors are composed of an elastomer substrate embedded with liquid metal-filled microchannels as the sensing element [5]. As the sensor deforms via strain, curvature or surface pressure, the cross-sectional area and length of the conductive fluid changes, thereby changing the resistance.

The goal of this paper is to identify the best method to create a desired microchannel size and geometry. The metric by which methods are compared will be their reproducibility—the similarity of microchannels produced by the same method. Additionally, the accuracy of a manufacturing method relative to the design geometry specified in the CAD model is presented.

2 Previous Work

An early example of a highly deformable sensor was developed by R. J. Whitney, in which mercury was enclosed inside of a rubber tube wrapped around a human leg [6]. One refinement of this technique embeds microchannels filled with eutectic gallium-indium alloy (eGaIn) or gallium-indium-tin alloy (Galinstan) within a stretchable silicone rubber substrate. In contrast to Whitney's work, the channels are patterned into bulk elastomer. Although various manufacturing techniques, described below, have been developed to form microchannels in an elastomer substrate, there has not been a rigorous study compar-

*Address all correspondence to this author.

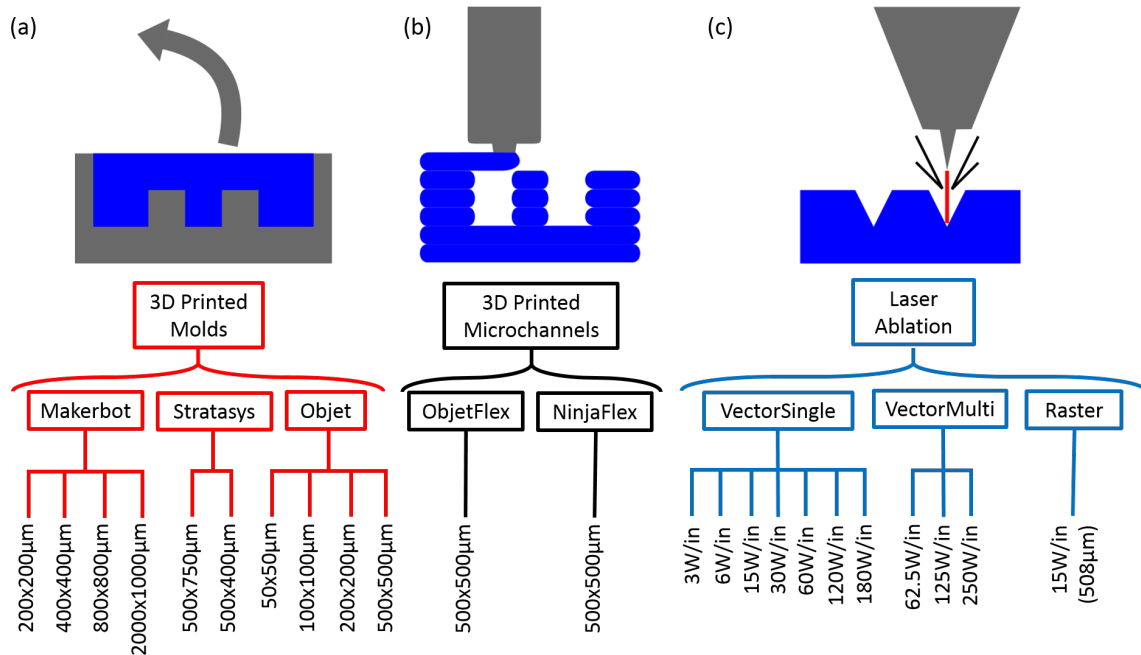


FIGURE 1: Overview of the methods and treatments included in this study. Channel dimensions as specified in CAD are listed for two methods: (a) 3D printed molds and (b) 3D printed microchannels. Energy levels are listed for (c) laser ablation. Prescribed channel width is specified for raster-mode laser manufacturing.

ing the performance of each of these methods, particularly at the micro- to millimeter scales. The cross-sectional geometry of microchannels has been shown to impact the functionality of the device [7]. This paper will explore manufacturing methods for creating embedded microchannels for large deformation sensors and determine each one's applicability to different microchannel geometries.

Researchers have developed many manufacturing techniques to make flexible circuits with microchannels. Techniques that were originally developed in the field of microfluidics [8–12] have been extended to create stretchable and flexible circuits and sensors composed of silicone elastomers, commonly PDMS (poly(dimethylsiloxane)) (Dow Corning Sylgard 184) or Ecoflex 00-30 (Smooth-On). A popular technique is to pour liquid prepolymer solution into a mold containing the negative of the desired features, i.e. raised features typically with rectangular cross-sections [13–15]. Molds for casting silicone elastomers are commonly formed using photolithography [16], e-beam lithography [17], and fused-deposition modeling [3]. Alternatively, etching techniques remove material through reactive ion etching [13, 18, 19] or laser ablation [20, 21] of PDMS. After forming the open channels in the substrate, the channels are capped by bonding to another polymer layer. This is typically accomplished in two ways: plasma bonding [1, 2, 13–15], and bonding uncured polymer to the patterned polymer [3, 22]. Microchannels

have also been formed using an additive manufacturing method, where diamond-shaped cross-sections were shown to eliminate the need for support material within the channel [23]. In order to create flexible electronic devices, conductive fluid may be injected into the pre-formed channels.

Alternate methods of creating flexible circuits with conductive liquid embedded in elastomer focus on first patterning the liquid, then encapsulating the trace in elastomer [24]. Researchers have encased conductive eGaIn-PDMS composite patterns inside of pure PDMS [25] and selectively wet eGaIn onto a substrate using masked deposition [26–28]. Using lithography-based techniques, eGaIn has been patterned via imprinting [29] and microcontact printing techniques [30]. Both inkjet [31] and 3D printing [32, 33] have also been used to pattern eGaIn on stretchable substrates. Others have combined the patterning and encapsulation steps by utilizing additive manufacturing techniques to extrude conductive fluid traces inside of liquid prepolymer [34] or co-extrude both the conductive fluid and the prepolymer together [35]. These alternate methods depart from the previously described molding and etching techniques by eliminating the need to create microchannels in the substrate.

Given all the manufacturing methods described above, this paper will assess the applicability of 3D printed molds, 3D printed microchannels and laser ablation for different microchannel geometries towards the purpose of liquid metal-embedded

elastomer circuits (Fig. 1). Molds composed of photoresist patterned on silicon wafers will not be reviewed in this paper as the processes required to fabricate precise features at the micro-scale have already been well-characterized [13–16]. Due to the required chemicals and equipment, photoresist patterning is a more complex and less accessible process relative to 3D printing. In contrast, fabricating 3D printed molds, as well as direct 3D printing and laser ablating microchannels, are cheaper, more easily iterated, and more suitable for larger scales.

3 Manufacturing Methods

Methods of manufacturing microchannels in silicone elastomer can be divided into three primary approaches: casting channels in a mold, directly manufacturing the microchannels by 3D printing elastomeric materials, and subtractively etching out the microchannels. In the molding and laser ablation manufacturing methods, all samples were manufactured using Smooth-Sil 950 (Smooth-On). Smooth-Sil 950 is an emerging material for deformable systems and has a Shore hardness of 50A, comparable to other soft robotics materials such as PDMS and Ecoflex 00-30 which have Shore hardnesses of 45A and 00-30, respectively [36]. Smooth-Sil 950 was chosen primarily for its opacity, lending itself well to imaging using a 3D optical surface profiler (Zeta-20, Zeta Instruments). The methods explored in this study are mapped in Fig. 1. Additionally, methods for processing microchannels into flexible electronic devices are detailed below for each method.

3.1 Casting elastomer substrates in 3D printed molds

In this study, 3D printed molds were created using fused deposition modeling (FDM) (Makerbot Replicator 2, ABS filament; Stratasys Dimension 1200, ABS filament) and polymer inkjet 3D printing (Objet Connex 350, VeroWhitePlus resin). A goal of this study was to determine minimum and maximum features sizes across the different manufacturing patterns. Therefore, microchannel features specified in Fig. 1a were printed in an array. A range of sizes was examined to determine the performance of 3D printed molding as a function of microchannel size. Channels examined in this quantitative part of the study had an aspect ratio (AR) of 1, with the exception of a $2000\mu\text{m}$ wide, $1000\mu\text{m}$ high (AR=0.5) channel printed using the Makerbot and both molds printed using the Stratasys. Since features with ARs less than 1 are more stable than higher ARs, it is assumed that the results of AR=1 channels can be used to inform low AR channel design. Higher AR channels (AR>1) were also studied to provide qualitative evaluations of 3D printer capabilities.

Prior to casting, each mold was sprayed with mold-release to facilitate removal of the cured polymer. Smooth-Sil 950 prepolymer was mixed at the supplier-recommended 10:1 ratio, poured into the mold and degassed in a vacuum chamber. The

polymer cured for >12 hours at 20°C , to ensure full crosslinking. Each sample was then removed from the mold and cleaned with a sequence of solvents: acetone, isopropanol, ethanol, and distilled water, to remove mold-release residue. Sensors and electronics can then be manufactured by capping these microchannels using any of the methods described in [1–3, 13–15, 22], filling channels with liquid conductor (ex: eGaIn) and inserting wires into the microchannels. Microchannels were characterized using a 3D optical surface profiler prior to capping the channels. Due to polymer overhang obscuring the open face of the channel, samples were sliced perpendicular to the channel orientation to image the full cross-section geometry. Each image was then processed in ImageJ to determine the cross-sectional area of the microchannel.

3.2 Direct 3D printing of microchannels

Direct 3D printed samples were produced using an FDM (Printbot Simple) method extruding a thermoplastic polyurethane filament (NinjaFlex) and a polymer inkjet method (Objet Connex 350) printing a rubbery elastomer resin (TangoBlack). The prototype strain sensors consisted of a serpentine pattern of channels embedded inside of a dogbone outline in this study. For both additive manufacturing methods, multiple specimens with the same dimensions were printed (Fig. 1b). Because the microchannels are already capped, in order to examine the microchannels, the sensors were sliced perpendicular to the channel orientation and imaged using a 3D optical profiler. Accuracy and reproducibility values were determined from measurements of cross-sections of these sensors.

The FDM printer extruded the NinjaFlex polymer filament to form the body without support material inside of the void microchannels. The microchannel geometry must be compatible with the ability of an FDM printer to print unsupported features: for example, if the microchannel is too wide, filament may not be able to bridge the gap and will collapse into the channel. In contrast, the polymer inkjet system deposits liquid resin droplets and UV-cures the part layer-by-layer. Since the polymer resin is deposited as a liquid, support material for the channels was necessary to produce the part. The resulting part was an elastomer body composed of TangoBlack elastomer embedded with microchannels composed of support material. The support material is difficult to remove from the part without compromising the TangoBlack body.

In order to complete fabrication of electronics and sensors from these microchannels, after printing, the NinjaFlex microchannels may be injected with eGaIn. Wires may be inserted into the ends of the microchannels to make electrical connections. In contrast, the polymer inkjetted sensors contain support material inside the microchannels and therefore cannot be filled with eGaIn. However, future work in printing either conductive support material or removing support material will allow sensor manufacture similar to that of the NinjaFlex sensors.

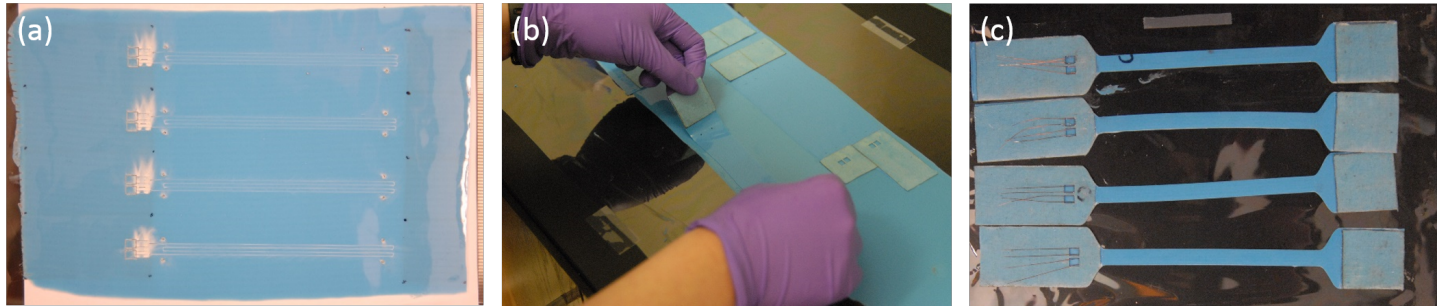


FIGURE 2: Fabrication of laser-ablated liquid metal embedded elastomer strain gauges with fabric end pads for interface robustness. (a) Laser-patterned elastomer sheet. (b) Tacky bonding a patterned sheet to a new sheet of elastomer. (c) Complete sensors, filled with eGaIn and with wires inserted into ports.

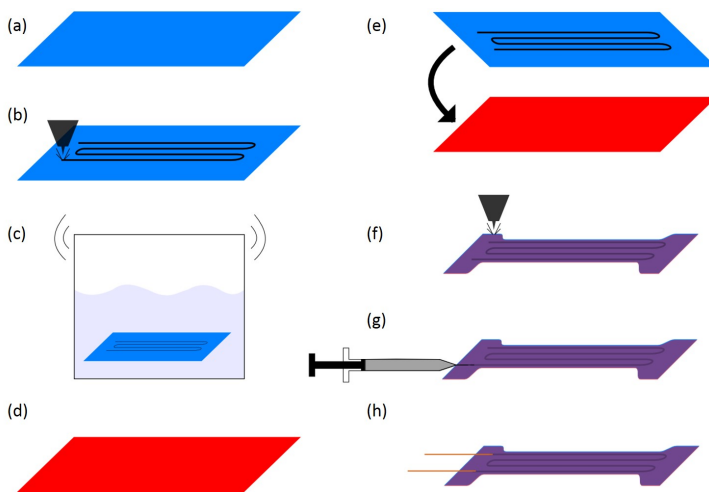


FIGURE 3: Fabrication of a liquid metal embedded elastomer strain gauge using laser manufacturing. (a) Rod-coat a sheet of elastomer. (b) Laser-etch microchannels into substrate. (c) Clean patterned substrate in a sonicator. (d) Rod-coat a 2nd sheet of elastomer. (e) Tacky bond the patterned sheet to the new sheet of elastomer. (f) Laser cut the outline of the sensor. (g) Filling microchannels with eGaIn using a syringe. (h) Insert and seal wires into sensor.

3.3 Subtractive manufacturing using laser ablation

In contrast to molding microchannel features into elastomer substrates, we have also etched the features using a laser ablation method (30W CO₂ laser; Universal Laser Systems VLS 2.30) in both raster and vector mode. The depth of features is defined by the amount of energy deposited into the substrate. Multiple energy levels were tested to examine the effect on microchannel size.

Prior to laser etching, elastomer substrates were prepared and cast using a rod coating technique in which uncured polymer is scraped across PET (polyethylene terephthalate) film using a threaded rod to control the thickness of the resulting substrate. Although we used rod-coating to form the substrate, any

solid substrate may be laser-etched. Once cured, the elastomer sheet is etched (Fig. 2a, 3b) and the resulting patterned sheet is then cleaned with toluene or acetone in a water bath sonicator (Bransonic 1800 Ultrasonic MH Cleaning Bath), then rinsed with isopropanol, ethanol, and distilled water to remove soot and other debris (Fig. 3c). The cleaning step is crucial to fabricate electronic devices, as debris will cause breakages in liquid metal traces. Channel geometries were imaged using a 3D optical surface profiler using the surface scanning function. A minimum of 8 cross sections along the length of the channels were measured for their area, depth and width in each image.

Sensor and electronics may be fabricated by capping the laser-etched microchannels, as previously described. However, due to possible debris buildup or chemical changes in the material, we have found that plasma bonding is unsuccessful near laser ablated features. Here, we have employed tacky bonding [37] (bonding the fully-cured patterned substrate to a partially cured unpatterned substrate) (Fig. 2b, 3e). It should be noted that bonding often results in stretching of the polymer, yielding a discrepancy between the actual size of the sensor and the design that must be accounted for by adding tolerances to the design drawings. Finally, the sensor may be cut out (Fig. 3f), the channels filled with liquid conductor (Fig. 3g), and the wires inserted into the microchannel terminals to interface with external hardware (Fig. 3h).

4 Results and Discussion

The performance metric by which the effectiveness of a manufacturing technique is measured is its reproducibility—how much variation there is within a treatment level of a specific method (Fig. 4). The amount of variation was measured across a minimum of 12 replicates of the same manufacturing technique. As the amount of variability across replicates increases, the measure of reproducibility of a manufacturing method decreases. For this study, a coefficient of variation of 10% is the maximum variability beyond which a manufacturing method is no longer ap-

Manufacturing method	Recommended range (μm^2)	Expected error	Expected variation
Laser Vector Single Pass	100 - 100,000	n/a	10.44%
Laser Vector Multi Pass	50,000 - 200,000	n/a	3.73%
Direct 3D Printing (Objet)	100,000 - 500,000	29.54%	6.77%
Casting in 3D Printed Molds	>100,000	31.10%	3.40%

TABLE 1: Recommended manufacturing methods based on desired microchannel cross-sectional areas. Lower expected error and expected variation refer to higher measures of accuracy and reproducibility, respectively. Laser vectored microchannels have triangular cross-sections; 3D printed and cast microchannels have rectangular cross-sections with $AR \leq 1$. The expected error for laser vectored channels is not an applicable value because channel dimensions are not directly prescribed prior to fabrication using laser ablation methods.

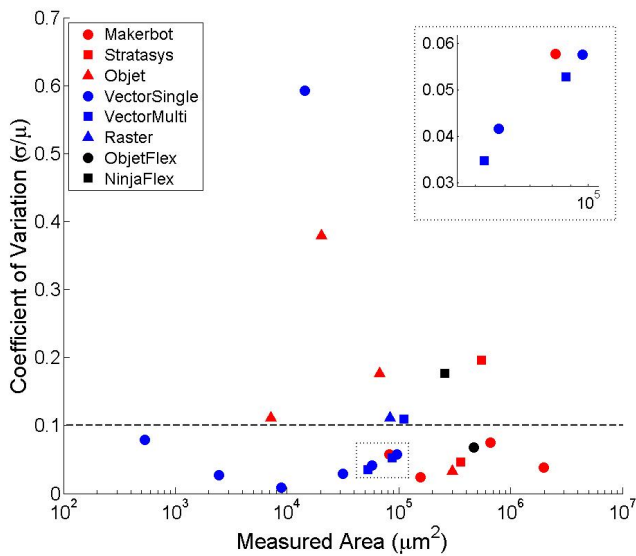


FIGURE 4: Reproducibility of microchannel size is represented as variation in cross-sectional area of multiple microchannel sizes for different manufacturing methods. A smaller variation indicates a higher degree of reproducibility. For reference, the dashed line indicates 10% variation, a threshold at which a manufacturing method may no longer be suitable for the desired cross-sectional area. A boxed inset has been inserted to clarify the position of overlapping points.

appropriate for the desired microchannel size. From Fig. 4 it is apparent that, in general, laser ablation is capable of repeatedly producing smaller microchannels, whereas 3D printed molding and additive manufacturing are not. In the instance of a particularly high variation value in channels created by a single-pass vectored laser-etched channel, there is a significant range both above and below this channel size in which the variation is below the 10% threshold. The recommended range for single-pass vectored laser etch thus does not reflect this singular point. This outlier is most likely due to inhomogeneity in the polymer or a failure to ensure flatness of the substrate prior to the etching procedure.

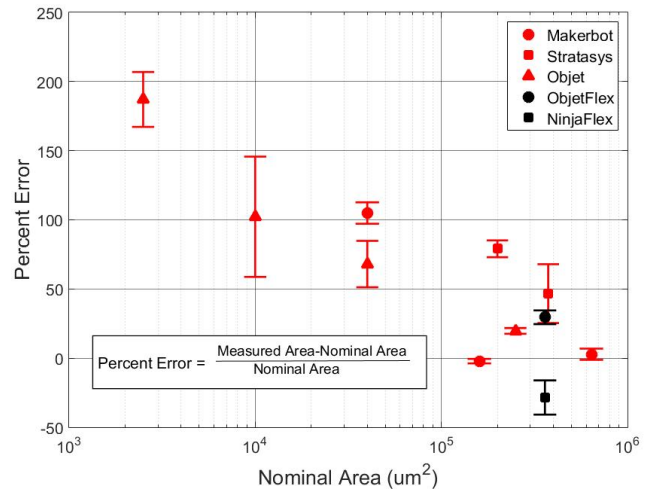


FIGURE 5: Accuracy of manufacturing methods indicated as percent error of experimental values of microchannel width compared to nominal dimensions specified in CAD models. Error bars indicate a 95% confidence interval. 0% error is indicative of a perfectly accurate manufacturing method. A positive percent error indicates a measured area larger than nominal dimensions, and vice versa for negative percent error. This plot contains data relevant to samples made from both 3D printed molds and additively manufactured microchannels.

cedure.

In addition to reproducibility, measures of accuracy—how closely the resulting microchannel conforms to the specified dimensions, are reported for the 3D printed molding and additive manufacturing techniques (Fig. 5). The width of the error bars in this plot are analogous to the coefficient of variation in Fig. 4. At smaller feature sizes, slight variations in printer operation will more severely decrease the accuracy of the part. These channel sizes are near the limit of printability due to the fixed size of the nozzle or spot size and the precision of its positioning.

Setting the maximum variability permissible to be 10%, as shown in Fig. 4, the appropriate manufacturing methods can be

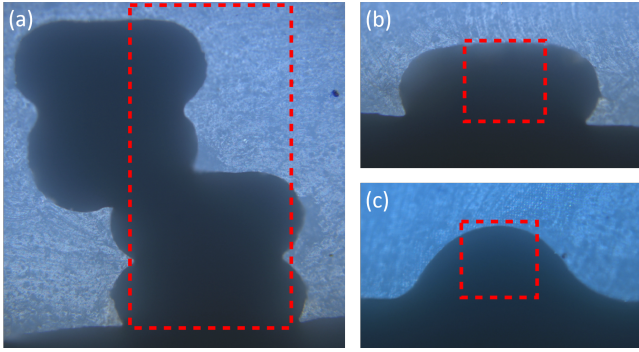


FIGURE 6: Microchannel cross-sections in which the actual channel deviates significantly from the original CAD design due to drawbacks of 3D printing manufacture. The issues demonstrated arise from (a) imprecise filament stacking, (b) filament overhang, and (c) polymer resin spreading. These issues result in molded microchannels that deviate heavily from the the red box overlaid onto the cross-section, indicating the CAD specification for the cross-sectional area. (a) Box: $400 \times 800 \mu\text{m}$. Printer: Makerbot Replicator 2. (b) Box: $200 \times 200 \mu\text{m}$. Printer: Makerbot Replicator 2. (c) Box: $200 \times 200 \mu\text{m}$. Printer: Objet Connex 350.

identified for a given range and are listed in Table 1. The expected error, shown in Fig. 5, of a manufacturing method (Table 1) should be factored into the design. If a method is highly reproducible, the level of inaccuracy will be consistent for every sample produced.

4.1 Casting elastomer substrates in 3D printed molds

As seen in the cross-sectional images (Fig. 6a, b), microchannel features created using the FDM printer suffer from two key deficiencies: void volume due to filament overhang and poor filament stacking/alignment. Both of these problems result in channels that deviate from the ideal rectangular cross-section. High aspect ratio features are difficult to accomplish using 3D printed molds due to poor alignment capabilities of FDM (Fig. 6a). Similar results occurred on $AR > 1$ parts printed with the Stratasys printer, contributing to a higher variability on $AR > 1$ parts when compared to $AR < 1$ parts. Furthermore, the void space between the widest part of the channel filament and the bottom surface of the mold creates thin protrusions in the cast polymer that may cause complications such as clots or collapse of the channel when bonding to a sealing sheet of elastomer (Fig. 6b). In contrast, microchannel features in polymer inkjetted molds present the opposite of overhang: spreading of resin (Fig. 6c). Though this results in a smooth casting of elastomer, smaller channel features may be lost due to the resin spreading across the surface of the part before it is solidified by exposure to the UV light.

As a result of these limitations, there is often significant in-

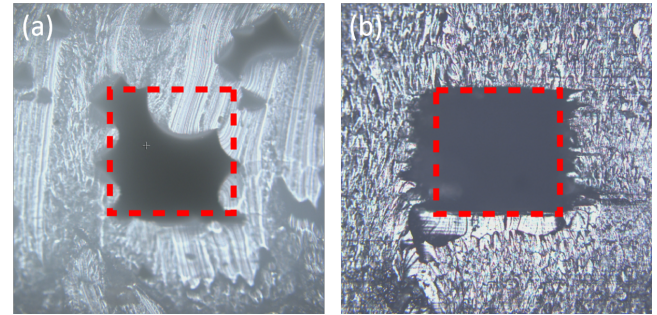


FIGURE 7: Images of the cross-section of microchannels created using (a) NinjaFlex printed in a Printbot, and (b) TangoPlus printed with an Objet Connex 350. The overlaid box indicates the nominal $500 \times 500 \mu\text{m}$ channel drawn in CAD.

accuracy when comparing the nominal area of the microchannel as specified in a CAD design to the area of the resulting molded microchannel, even at $AR=1$. At smaller microchannel geometries, the percent errors can range to nearly 200% (Fig. 5). Moreover, there is a hard limit on the smallest printable trace for each 3D printer. For example, Makerbot Replicator 2 printers are incapable of printing microchannels with a CAD dimension of $50 \times 50 \mu\text{m}$. The smallest microchannels attempted were printed with an Objet Connex 350 as it is capable of printing traces of height $30 \mu\text{m}$ and with a precision of $\pm 5 \mu\text{m}$, as specified by the manufacturer. Larger features ($\geq 100 \mu\text{m}$) were printed using a Makerbot Replicator 2, which has a rated $100 \mu\text{m}$ layer resolution and an x - y precision of $11 \mu\text{m}$, also specified by the manufacturer.

While the percent error may be quite large for some channel sizes, 3D printing may still be a viable option as long as the amount of variation is within design thresholds. A designer may account for the known level of inaccuracy expected for a certain 3D printer printing a specific channel size. For both the Objet and Makerbot molds, as the feature size is increased, there is a clear decrease in both percent error and variability, as evidenced by smaller confidence intervals around each point (Fig. 5) and decreasing coefficient of variation (Fig. 4).

4.2 Direct 3D printing of microchannels

The NinjaFlex and ObjetFlex sensors displayed -28.47% and 29.54% deviations from the intended geometry (Fig. 5). Since the NinjaFlex filament collapsed into the void microchannels, the measured cross-section was smaller than the nominal dimensions (Fig. 7a). Conversely, due to resin spread of the support material, the microchannels printed with the Objet were larger than the nominal dimensions (Fig. 7b). In terms of reproducibility, the ObjetFlex sensors had a much lower variability in microchannel geometry, due to the presence of support material (Fig. 4). This is expected because the NinjaFlex sensors are being printed without support material, hence, it is reasonable to

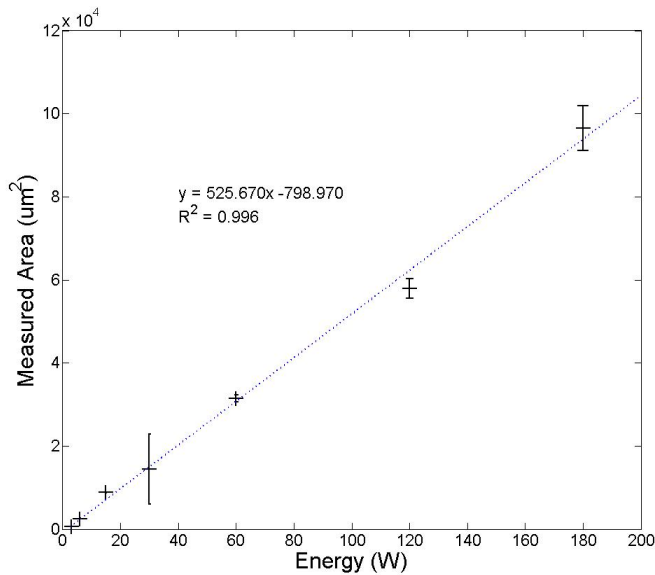


FIGURE 8: Cross-sectional areas of single-pass, laser-etch vectored channels. Error bars indicate 95% confidence interval for the area. The dotted line indicates the linear relationship between the amount of energy deposited into the material and the resulting cross-sectional area.

assume that some of the extruded filament will sink into the void as it is printed, as shown in Fig. 7a. As a result, the size of the microchannels produced by printing NinjaFlex varies greatly from sensor to sensor.

4.3 Subtractive manufacturing using laser ablation

The geometry of microchannels created using laser ablation are dependent on the amount of energy deposited by the laser into the material. For example, the power density output of our 30W laser is calculated as $\%Power * 30W/in$. Due to multiple pulses hitting the same spot on the substrate, the energy entering the substrate per unit length is calculated as $\frac{\%Power}{\%Speed} * 30W/in$. While these equations are specific to the VLS 2.30 laser system used in this paper, other laser cutting systems have similar means of controlling energy input into the material. Fig. 8 illustrates the linearity of the relationship between the energy deposited and the resulting cross-sectional area. As energy levels increase, the confidence interval around the expected cross-sectional area is generally larger due to increased soot deposition on the material, compromising the effectiveness of the laser. Variations can arise from non-uniform heat diffusion within the material due to non-homogeneous compositions or varying substrate thicknesses.

The cross-section of a typical vectored microchannel is triangular, as seen in Fig. 9b. As such, high aspect ratio rectangular cross-section channels are difficult to accomplish using the laser. Attempts to create high aspect ratio features involve sub-

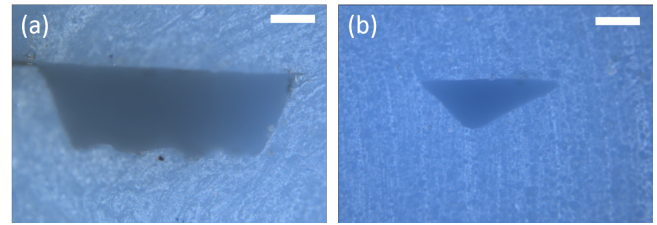


FIGURE 9: Cross-sections of a) rastered, and b) vectored channels that have been capped with a second layer. The laser settings for both channels are 25% power and 50% speed. Scale bar is 100μm.

jecting the material to multiple passes of the laser. However, issues arise when soot and debris from previous cuts occlude the path of the laser, rendering subsequent passes less effective at removing material. Scaling the amount of ablation by the number of passes is inaccurate due to reduced energy transfer for subsequent passes. Additionally, since the soot accumulation is non-uniformly distributed across the surface due to its particulate nature, the resulting etch has a much rougher surface and a less uniform cross-section. Theoretically, the soot could be cleaned out of the channels in between multiple passes, however, realignment with previous cuts will add error into the process. Therefore, ideally, subtractive manufacturing of microchannels requires a single pass across the substrate.

In addition to vectoring, the laser also operates in a rastering mode (Fig. 9). Vectoring is used for single-pass lines to be etched partially or cut fully through the material; rastering is used for large area patterning. In raster mode, the area to be etched is defined, however, the depth remains a function of the laser's operating parameters and the material properties. Rastering may be used to create channels wider than those produced by vectoring, however, the channel surface may be rougher and less uniform and the time to produce a channel is much longer. The accuracy of a raster cut can be determined by comparing the actual width of a channel to the design width. To test the accuracy of a raster cut, a rastered channel was measured using the optical profiler. The specified channel width was 508μm. The 95% confidence interval of the actual width was $540.644 \pm 17.599 \mu m$, with an average percent error of 6.42% and a coefficient of variation of 3.26%.

The vectoring results presented in Fig. 8 can be translated to the expected size of the rastered channel. The expected rastered channel cross-sectional area (A_r) can be calculated from a vectored area (A_v) for the same laser energy level:

$$A_r = A_v * \frac{w * PPI + 1}{2},$$

where w is the channel width specified in the vector graphic illustration and PPI is the pulses per inch fired by the laser. This

equation assumes half the width of one pulse overlaps with half of the adjacent pulses. For example, in Fig. 9, the rastered channel has an average area of $82879.09\mu\text{m}^2$; the vectored area has an average area of $7933.32\mu\text{m}^2$. The width of the channel was prescribed to be $508\mu\text{m}$ or 0.02in . Substituting these values into the above equation, the theoretical A_r is $83299.98\mu\text{m}^2$, which is a 0.5% error compared to the actual area of $82879.09\mu\text{m}^2$. Therefore, once the area of a channel from a single vectored pass of the laser is known, the approximate area of a rastered channel can be determined.

5 Conclusion

In this paper, methods of patterning microchannels into silicone elastomers for highly deformable sensors were compared to determine which manufacturing technique is most appropriate for a given cross-sectional area. Studies were performed for three manufacturing techniques: casting microchannels in 3D printed molds, laser ablation of microchannels, and 3D printing the substrate with embedded void microchannels. Both the reproducibility and accuracy of these techniques were determined. Using these values as metrics for the compatibility for various channel geometries, recommended manufacturing techniques are prescribed for ranges of channel geometry sizes. By employing more compatible manufacturing techniques, fabrication of liquid metal-embedded elastomer sensing and electrical devices may be tuned for increased yield and increased reliability.

6 Acknowledgments

The authors would like to thank Dr. J. William Boley, R. Adam Bilodeau, Edward White, and Jennifer Case for their input and sensor manufacturing insights. The authors would also like to thank Trevor Lear for assistance with microchannel measurements. Lastly, the authors would like to thank Prof. Thomas Siegmund and Ying Long Chen for their assistance with the Objet 3D printer. This work was supported by an Early Career Faculty grant NNX14A052G from NASA's Space Technology Research Grants Program. MCY is supported by the National Science Foundation Graduate Research Fellowship (Grant DGE-1333468). Any opinion, findings, and conclusions or recommendations expressed in this material are those of the authors and do not necessarily reflect the views of the National Aeronautics and Space Administration or the National Science Foundation.

REFERENCES

[1] Kramer, R. K., Majidi, C., Sahai, R., and Wood, R. J., 2011. "Soft curvature sensors for joint angle proprioception". In *Intelligent Robots and Systems (IROS)*, 2011 IEEE/RSJ International Conference on, pp. 1919–1926.

[2] Park, Y.-L., Majidi, C., Kramer, R., Brard, P., and Wood, R. J., 2010. "Hyperelastic pressure sensing with a liquid-embedded elastomer". *Journal of Micromechanics and Microengineering*, **20**(12), Dec., p. 125029.

[3] Meng, Y., Park, Y.-L., Pei, H., Vogt, D., Aubin, P. M., Winchell, E., Fluke, L., Stirling, L., Wood, R. J., and Walsh, C. J., 2014. "Wearable soft sensing suit for human gait measurement". *The International Journal of Robotics Research*, **33**(14), Dec., pp. 1748–1764.

[4] Majidi, C., Kramer, R., and Wood, R. J., 2011. "A non-differential elastomer curvature sensor for softer-than-skin electronics". *Smart Materials and Structures*, **20**(10), Oct., p. 105017.

[5] Dickey, M. D., 2014. "Emerging Applications of Liquid Metals Featuring Surface Oxides". *ACS Appl. Mater. Interfaces*, Oct.

[6] Whitney, R. J., 1953. "The measurement of volume changes in human limbs". *The Journal of physiology*, **121**(1), pp. 1–27.

[7] Park, Y.-L., Tepayotl-Ramirez, D., Wood, R. J., and Majidi, C., 2012. "Influence of cross-sectional geometry on the sensitivity and hysteresis of liquid-phase electronic pressure sensors". *Applied Physics Letters*, **101**(19), Nov., p. 191904.

[8] McDonald, J. C., Chabinyk, M. L., Metallo, S. J., Anderson, J. R., Stroock, A. D., and Whitesides, G. M., 2002. "Prototyping of Microfluidic Devices in Poly(dimethylsiloxane) Using Solid-Object Printing". *Anal. Chem.*, **74**(7), Apr., pp. 1537–1545.

[9] Chan-Park, M. B., Zhang, J., Yan, Y., and Yue, C. Y., 2004. "Fabrication of large SU-8 mold with high aspect ratio microchannels by UV exposure dose reduction". *Sensors and Actuators B: Chemical*, **101**(12), June, pp. 175–182.

[10] Chossat, J.-B., Park, Y.-L., Wood, R., and Duchaine, V., 2013. "A Soft Strain Sensor Based on Ionic and Metal Liquids". *IEEE Sensors Journal*, **13**(9), Sept., pp. 3405–3414.

[11] Jeon, N. L., Chiu, D. T., Wargo, C. J., Wu, H., Choi, I. S., Anderson, J. R., and Whitesides, G. M., 2002. "Microfluidics Section: Design and Fabrication of Integrated Passive Valves and Pumps for Flexible Polymer 3-Dimensional Microfluidic Systems". *Biomedical Microdevices*, **4**(2), May, pp. 117–121.

[12] Plecis, A., and Chen, Y., 2007. "Fabrication of microfluidic devices based on glass/PDMS/glass technology". *Microelectronic Engineering*, **84**(58), May, pp. 1265–1269.

[13] Jo, B.-H., Van Lerberghe, L., Motsegood, K., and Beebe, D., 2000. "Three-dimensional micro-channel fabrication in polydimethylsiloxane (PDMS) elastomer". *Journal of Microelectromechanical Systems*, **9**(1), Mar., pp. 76–81.

[14] Xia, Y., and Whitesides, G. M., 1998. "Soft Lithography". *Angewandte Chemie International Edition*, **37**(5), Mar., pp. 550–575.

[15] Xia, Y., and Whitesides, G. M., 1998. "Soft Lithography". *Annual Review of Materials Science*, **28**(1), pp. 153–184.

[16] Folch, A., Ayon, A., Hurtado, O., Schmidt, M. A., and Toner, M., 1999. "Molding of Deep Polydimethylsiloxane Microstructures for Microfluidics and Biological Applications". *J Biomech Eng*, **121**(1), Feb., pp. 28–34.

[17] Quake, S. R., and Scherer, A., 2000. "From Micro- to Nanofabrication with Soft Materials". *Science*, **290**(5496), Nov., pp. 1536–1540.

[18] Garra, J., Long, T., Currie, J., Schneider, T., White, R., and Paranjape, M., 2002. "Dry etching of polydimethylsiloxane for microfluidic systems". *Journal of Vacuum Science & Technology A*, **20**(3), May, pp. 975–982.

[19] Balakrishnan, B., Patil, S., and Smela, E., 2009. "Patterning PDMS using a combination of wet and dry etching". *Journal of Micromechanics and Microengineering*, **19**(12), Dec., p. 125029.

- chanics and Microengineering*, **19**(4), Apr., p. 047002.
- [20] Wolfe, D. B., Ashcom, J. B., Hwang, J. C., Schaffer, C. B., Mazur, E., and Whitesides, G. M., 2003. "Customization of poly (dimethylsiloxane) stamps by micromachining using a femtosecond-pulsed laser". *Advanced Materials*, **15**(1), pp. 62–65.
- [21] Fogarty, B. A., Heppert, K. E., Cory, T. J., Hulbutta, K. R., Martin, R. S., and Lunte, S. M., 2005. "Rapid fabrication of poly(dimethylsiloxane)-based microchip capillary electrophoresis devices using CO₂ laser ablation". *The Analyst*, **130**(6), pp. 924–930.
- [22] Unger, M. A., Chou, H.-P., Thorsen, T., Scherer, A., and Quake, S. R., 2000. "Monolithic Microfabricated Valves and Pumps by Multilayer Soft Lithography". *Science*, **288**(5463), Apr., pp. 113–116.
- [23] Swensen, J. P., Odhner, L. U., Araki, B., and Dollar, A. M., 2015. "Printing three-dimensional electrical traces in additive manufactured parts for injection of low melting temperature metals". *J. Mechanisms Robotics*, **7**(2), May, pp. 021004–021004.
- [24] Joshupura, I. D., Ayers, H. R., Majidi, C., and Dickey, M. D., 2015. "Methods to pattern liquid metals". *J. Mater. Chem. C*, **3**(16), pp. 3834–3841.
- [25] Lu, T., Finkenauer, L., Wissman, J., and Majidi, C., 2014. "Rapid Prototyping for Soft-Matter Electronics". *Adv. Funct. Mater.*, Feb., pp. 3351–3356.
- [26] Kramer, R. K., Majidi, C., and Wood, R. J., 2013. "Masked Deposition of Gallium-Indium Alloys for Liquid-Embedded Elastomer Conductors". *Advanced Functional Materials*, **23**(42), Nov., pp. 5292–5296.
- [27] Jeong, S. H., Hagman, A., Hjort, K., Jobs, M., Sundqvist, J., and Wu, Z., 2012. "Liquid alloy printing of microfluidic stretchable electronics". *Lab Chip*, **12**(22), Nov., pp. 4657–4664. WOS:000310865200010.
- [28] Jeong, S. H., Hjort, K., and Wu, Z., 2015. "Tape Transfer Atomization Patterning of Liquid Alloys for Microfluidic Stretchable Wireless Power Transfer". *Sci. Rep.*, **5**, Feb.
- [29] Gozen, B. A., Tabatabai, A., Ozdoganlar, O. B., and Majidi, C., 2014. "High-Density Soft-Matter Electronics with Micron-Scale Line Width". *Adv. Mater.*, **26**(30), Aug., pp. 5211–5216.
- [30] Tabatabai, A., Fassler, A., Usiak, C., and Majidi, C., 2013. "Liquid-Phase Gallium-Indium Alloy Electronics with Microcontact Printing". *Langmuir*, **29**(20), May, pp. 6194–6200.
- [31] Boley, J. W., White, E. L., and Kramer, R. K., 2015. "Mechanically Sintered Gallium-Indium Nanoparticles". *Adv. Mater.*, **27**(14), Apr., pp. 2355–2360.
- [32] Ladd, C., So, J.-H., Muth, J., and Dickey, M. D., 2013. "3d Printing of Free Standing Liquid Metal Microstructures". *Adv. Mater.*, **25**(36), Sept., pp. 5081–5085.
- [33] Boley, J. W., White, E. L., Chiu, G. T.-C., and Kramer, R. K., 2014. "Direct Writing of Gallium-Indium Alloy for Stretchable Electronics". *Adv. Funct. Mater.*, **24**(23), June, pp. 3501–3507.
- [34] Muth, J. T., Vogt, D. M., Truby, R. L., Meng, Y., Kolesky, D. B., Wood, R. J., and Lewis, J. A., 2014. "Embedded 3d Printing of Strain Sensors within Highly Stretchable Elastomers". *Advanced Materials*, June, pp. 6307–6312.
- [35] Frutiger, A., Muth, J. T., Vogt, D. M., Meng, Y., Campo, A., Valentin, A. D., Walsh, C. J., and Lewis, J. A., 2015. "Capacitive Soft Strain Sensors via Multicore-Shell Fiber Printing". *Advanced Materials*, Feb., pp. 2440–2446.
- [36] Case, J. C., White, E. L., and Kramer, R. K., 2015. "Soft Material Characterization for Robotic Applications". *Soft Robotics*, **2**(2), June, pp. 80–87.
- [37] Eddings, M. A., Johnson, M. A., and Gale, B. K., 2008. "Determining the optimal PDMS/PDMS bonding technique for microfluidic devices". *Journal of Micromechanics and Microengineering*, **18**(6), June, p. 067001.